Letter

A Data-Driven Real-Time Trajectory Planning and Control Methodology for UGVs Using LSTMRDNN

Kaiyuan Chen, *Member, IEEE*, Runqi Chai, *Senior Member, IEEE*, Runda Zhang, Zhida Xing, Yuanqing Xia, *Fellow, IEEE*, and Guoping Liu, *Fellow, IEEE*

Dear Editor,

This letter presents a novel data-driven trajectory planning and control scheme for the unmanned ground vehicles (UGVs). A recent work [1] has demonstrated the effectiveness of approximating the optimal state feedback for a nonlinear unmanned system via deep neural network (DNN). To further the previous research, we construct a long-short term memory recurrent deep neural network (LSTMRDNN) to improve the performance of the data-driven approximation instrument. The proposed strategy is evaluated and verified through theoretical analyses and experiments.

Trajectory planning and control of unmanned systems remain topical. Traditional solutions include sample-and-search methods [2], optimization-based methods [3] and others. Sample-and-search methods (such as A* [4], RRT [5], and their derivative algorithms [6]) are commonly engaged for their low computational burden. In recent years, optimization-based planning and control strategies have attracted ever more interest, as the environmental factors and task targets can be adhered to the algorithms. Wang *et al*. [7] solved the trajectory problem of underactuated autonomous vehicles using a neural dynamics optimization-based approach. Wang *et al*. [8] proposed a novel periodic motion plan for underactuated autonomous vehicles based on optimization search. Hu *et al*. [9] used probabilistic decision-making method combined with trajectory optimization to solve the problem of vehicle lane changing in automatic driving. However, the high computational complexity and the high dependence on onboard hardware remain issues. To address the drawbacks, artificial intelligence theory based trajectory optimization schemes are developed for the optimal landing of spacecraft [10], online trajectory planning and control of hypersonic vehicles [1] and the trajectory planning and tracking control of UGVs [11].

Nevertheless, there is still room for improvement on the performance of the planning and control scheme. Furthermore, in the previous stability analyses of neural network controllers, stability was ensured by employing either an adaptive control framework [12] or methods based on predefined Lyapunov functions [13], [14] for real-time adjustment of network weights. However, the aforementioned techniques are only applicable to controllers based on shallow neural networks. When confronted with the deep learning network models commonly used in most research, difficulties are often witnessed in formulating adaptive rules and finding appropriate Lyapunov functions.

The main contributions of the research presented in the letter are: first, a robust data-driven based real time motion planning scheme for UGVs is proposed, of which an improved performance with minimal computational overhead compared to the existing main stream optimization-based methods is validated. The proposed method has high accuracy and is completely close to the optimal trajectory. Second, the stability of the states of trajectory obtained through the proposed motion planner with the consideration of initial state perturbations is theoretically analyzed with the help of differential algebra and high-order Taylor maps (HOTMs), which is further verified in experiments.

Problem formulation: The main purpose of the study is to testify and verify the proposed UGV trajectory optimization scheme. Therefore, a model of the UGV, the scenario and the optimal control problem need to be established.

Based on the physical characteristics of the UGV in the research, the kinematic model can be described as follows:

$$\begin{aligned} &\dot{p}_x(t) = v(t)\cos(\theta(t)) \quad \dot{v}(t) = a(t) \quad \dot{\theta}(t) = v(t)\tan(\phi(t))/l \\ &\dot{p}_y(t) = v(t)\sin(\theta(t)) \quad \dot{a}(t) = \eta(t) \quad \dot{\phi}(t) = \omega(t). \end{aligned} \tag{1}$$

Among them, the system state is $\boldsymbol{x} = [p_x, p_y, v, a, \theta, \phi]^T$; the mathematical symbols within the brace represent the abscissa and ordinate of the rear wheel axis of the UGV, vehicle speed, acceleration, body direction angle and vehicle steering angle, respectively. The control values of the system include jerk and steering angle rate, which are included in $\boldsymbol{u} = [\eta, \omega]^T$. The state $\boldsymbol{x}$ and control $\boldsymbol{u}$ of the vehicle should be within a certain range

$$\boldsymbol{x}_{\min} \le \boldsymbol{x} \le \boldsymbol{x}_{\max}, \quad \boldsymbol{u}_{\min} \le \boldsymbol{u} \le \boldsymbol{u}_{\max}. \tag{2}$$

The movement of the UGV starts from the initial state $\boldsymbol{x}_0$ and finally terminates at the goal state $\boldsymbol{x}_f$

$$\boldsymbol{x}(t_0) = \boldsymbol{x}_0, \quad \boldsymbol{x}(t_f) = \boldsymbol{x}_f. \tag{3}$$

Another constraint of the motion planning task is collision-avoidance, which can be described as

$$vehicle\_func(\boldsymbol{x}) \cap Obs = \emptyset \tag{4}$$

where $vehicle\_func(\cdot)$ represents the mapping function of the vehicle state and the chassis, and Obs represents the collection of the obstacles in a certain scenario. The collision-avoidance constraint is then formulated in accordance with the method proposed in [15].

With the optimal objective set to the total task time, the optimal control problem is formulated as

$$\begin{aligned} &\min J = t_f \\ &\text{s.t. } \forall t \in [t_0, t_f] \\ &\quad (1) \quad \text{(dynamic constraints)} \\ &\quad (2) \quad \text{(state/control constraints)} \\ &\quad (3) \quad \text{(initial/terminal conditions)} \\ &\quad (4) \quad \text{(collision avoidance constraints).} \end{aligned} \tag{5}$$

Methodology: The framework of the proposed LSTMRDNN motion planning and control scheme is shown in Fig. 1. The upper part of the figure represents the training process, utilizing the double-layer desensitization trajectory optimization algorithm mentioned in [15] to solve the trajectory optimization model (5) in this design. A dataset is constructed based on the computed time-shortest optimal trajectory. This dataset comprises state and control variables representing optimal trajectories planned from different initial states, which have been normalized for subsequent network training. A specific sequence length is selected, with the state variable sequence of that length serving as the input for the LSTMRDNN, and the corresponding control variables as the network's output. Subsequently, the adaptive moment estimation (Adam) algorithm is employed to minimize the mean squared error (MSE) in training the LSTMRDNN to establish a mapping relationship between the vehicle state, denoted as $\boldsymbol{x}$, and the optimal control values, denoted as $\boldsymbol{u}^*$. The lower part of the figure is the working process of the neurocontroller, the optimal control value can be obtained in real time by inputting the vehicle state at the same time node to the neural network.

To theoretically analyze the stability of the states of trajectory obtained through the proposed controller with the consideration of initial state perturbations, differential algebra techniques and HOTMs are engaged. Using differential algebraic techniques as a foundation, we obtain a high-order Taylor expansion form for the solutions gen-

Corresponding author: Runqi Chai.

Citation: K. Chen, R. Chai, R. Zhang, Z. Xing, Y. Xia, and G. Liu, "A data-driven real-time trajectory planning and control methodology for UGVs using LSTMRDNN," *IEEE/CAA J. Autom. Sinica*, vol. 11, no. 5, pp. 1292–1294, May 2024.

The authors are with the Vanke School of Public Health, Institute for Healthy China, Tsinghua University, Beijing 100084, the School of Automation, Beijing Institute of Technology, Beijing 100081, and the Department of Electronic and Electrical Engineering, Southern University of Science and Technology, Shenzhen 518055, China (e-mail: kaiyuanchen@mail.tsinghua.edu.cn; r.chai@bit.edu.cn; runda.zhang@bit.edu.cn; xzd3120230854@bit.edu.cn; xia_yuanqing@bit.edu.cn; liugp@sustech.edu.cn).

Color versions of one or more of the figures in this paper are available online at http://ieeexplore.ieee.org.

Digital Object Identifier 10.1109/JAS.2024.124269

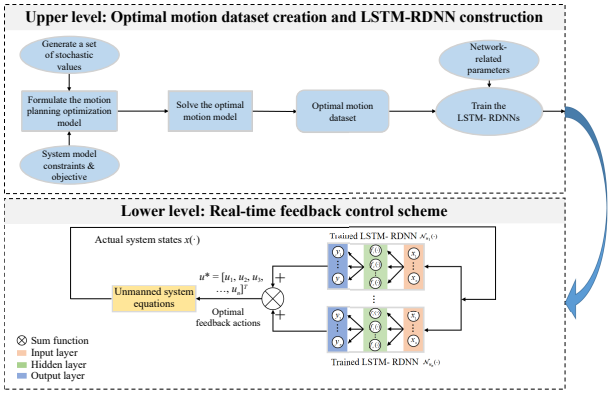

Fig. 1. Motion planning and control framework based on LSTMRDNN.

erated by the neural controller within the vicinity of the reference solution. This expansion is used for further analyzing the global behavior of the controller in the presence of initial state uncertainties.

We use $\mathcal{N}(\boldsymbol{x})$ to represent the mapping relations of the state-control pair. $\mathcal{N}(\boldsymbol{x}) \approx \boldsymbol{u}^*(\boldsymbol{x})$ is used to approximate the optimal state feedback control. As shown in Fig. 2, n networks $\mathcal{N}_i(\cdot)$ are used to learn the mapping relationship between each control quantity and state quantity separately.

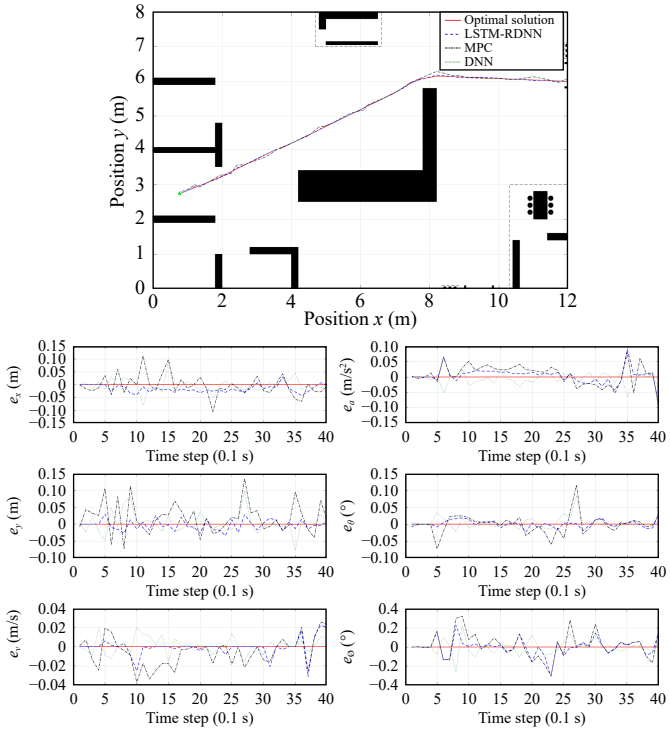

Fig. 2. Comparison results of trajectories generated by LSTMRDNN, DNN, MPC, and optimal trajectories.

$\boldsymbol{x}_0$ represents the initial state of the reference solution, the optimal trajectory generated from the neural network control is presented as

$$\boldsymbol{x}_{\mathcal{N}}(t) = \Psi_{\mathcal{N}}(\boldsymbol{x}_0, t). \tag{6}$$

By using differential algebra techniques and higher-order Taylor expansions, the solution under the initial condition $\boldsymbol{x}_0 + \delta\boldsymbol{x}_0$ can be obtained and expressed in its k-order Taylor expansion form

$$\boldsymbol{x}_{\mathcal{N}}(t) \approx \mathcal{M}_k^t(\delta\boldsymbol{x}_0). \tag{7}$$

Differential algebra technology is applied by introducing a new data type, which enables the computer program to output the Taylor expansion of the selected input. Subsequently, the trajectory approximation of the vehicle dynamics system under the initial condition $\boldsymbol{x}_0 + \delta\boldsymbol{x}_0$ is obtained through Runge-Kutta-Fehlberg numerical integration method. This is an explicit expression of the trajectory, which ensures convergence when the disturbance size $\delta\boldsymbol{x}_0$ of the initial condition is limited to the sphere $\mathcal{Q}_\varepsilon$ with a radius of ε.

The following equation describes the k-order Taylor expansion of the initial disturbance $\delta\boldsymbol{x}_0$ under each t:

$$\delta\boldsymbol{x}(t) = \mathcal{M}_k^t(\delta\boldsymbol{x}_0) - \Psi_{\mathcal{N}}(\boldsymbol{x}_0, t). \tag{8}$$

We use H_i to describe its tensor matrix expanded in the i-th order, for example, when $i = 1$, H_1 represents the gradient; When $i = 2$, H_2 represents the Hessian matrix.

Theorem 1: The convergence of the series in (8) is guaranteed for any $\delta\boldsymbol{x}_0$ belonging to the sphere $\mathcal{Q}_\varepsilon$, if $\lim_{k\to\infty} \frac{|a_{k+1}|}{|a_k|}$ exists where $a_k = \|H_k\|$. In that case, ε must satisfy the inequality $\varepsilon \lim_{k\to\infty} \frac{|a_{k+1}|}{|a_k|} < 1$.

Proof: First, write the i-th component of $\delta\boldsymbol{x}(t) = \mathcal{M}_k^t(\delta\boldsymbol{x}_0) - \Psi_{\mathcal{N}}(\boldsymbol{x}_0, t)$, using the Einstein notation

$$\delta x_i = h_{1,ij}\delta x_{0j} + h_{2,ijk}\delta x_{0j}\delta x_{0k} + h_{3,ijkl}\delta x_{0j}\delta x_{0k}\delta x_{0l} + \cdots \tag{9}$$

where δx_{0i} denotes the i-th component of $\delta\boldsymbol{x}_0$. The terms h_1, h_2 and h_3 are components of the Jacobian, the Hessian, and the third-order partial derivative tensors. Taking the norm of the above formula and using the induced matrix norm inequality and triangular inequality, we can get

$$\|\delta\boldsymbol{x}\| \le \|H_1\|\|\delta\boldsymbol{x}_0\| + \|H_2\|\|\delta\boldsymbol{x}_{02}\| + \|H_3\|\|\delta\boldsymbol{x}_{03}\| + \cdots \tag{10}$$

where $H_{2,ij} = h_{2,ikl}$ and $H_{3,ij} = h_{3,iklq}$ with $k = (j-1) \bmod n+1$, $l = (j-1)/n+1$ and $q = (j-1)/n^2+1$, $j = 1,2,3,\ldots,n^2$ and $j = 1,2,3,\ldots,n^3$ for each matrix. In order to write in matrix form, we have unfolded the tensors. We use the same method to the vectors $\delta\boldsymbol{x}_{02}$ and $\delta\boldsymbol{x}_{03}$ as $\delta x_{02,j} = \delta x_{0k}\delta x_{0l}$, $\delta x_{03,j} = \delta x_{0k}\delta x_{0l}\delta x_{0q}$. Therefore, $\|\delta\boldsymbol{x}_{02}\| = \|\delta\boldsymbol{x}_0\|^2$, $\|\delta\boldsymbol{x}_{03}\| = \|\delta\boldsymbol{x}_0\|^3$ under any r-norm. The size of $\delta\boldsymbol{x}$ can be limited

$$\|\delta\boldsymbol{x}\| \le a_1\|\delta\boldsymbol{x}_0\| + a_2\|\delta\boldsymbol{x}_0\|^2 + a_3\|\delta\boldsymbol{x}_0\|^3 + \cdots \tag{11}$$

where $a_k = \|H_k\|$.

As a consequence, for each $\delta\boldsymbol{x}_0$, such that $\|\delta\boldsymbol{x}_0\| < \varepsilon$, the following holds:

$$\|\delta\boldsymbol{x}\| < \sum_{i=0}^{k} a_i\varepsilon^i. \tag{12}$$

Applying the ratio test (base on D'Alembert's criterion), we could guarantee its absolute convergence whenever $\varepsilon \lim_{k\to\infty} \frac{|a_{k+1}|}{|a_k|} < 1$. ■

From Theorem 1, it can be observed that when the conditions outlined in Theorem 1 are met, (8) can converge. This ensures that the planned trajectory under the neural controller converges to the reference trajectory (reference solution). Consequently, trajectories planned based on the neural controller can also reach the final target state.

Theorem 2: The equilibrium point (the final target state) $\boldsymbol{x}_f = \lim_{t\to\infty} \Psi_{\mathcal{N}}(\boldsymbol{x}_0, t)$ is asymptotically stable for any perturbation $\delta\boldsymbol{x}_0 \in \mathcal{Q}_\varepsilon$ if and only if $\|H_k\| \longrightarrow 0$, $\forall k$, as $t \longrightarrow \infty$.

Proof: Assuming that $\boldsymbol{x}_f$ is asymptotically stable, then $\delta\boldsymbol{x}(t) \longrightarrow 0$, hence $\|H_k\| \longrightarrow 0$ $\forall k$. On the other hand, assuming that $\|H_k\| \longrightarrow 0$ $\forall k$ in the limit $t \longrightarrow \infty$, then we could find $\delta\boldsymbol{x}(t) \longrightarrow 0$ form (8), hence $\mathcal{M}_k^t(\delta\boldsymbol{x}_0) \longrightarrow \Psi_{\mathcal{N}}(\boldsymbol{x}_0, \infty) = \boldsymbol{x}_f$. ■

Experimental results: The scenario setting of the study is an evacuation task in a nursing home. The map was established based on the real scene of a nursing home. The task goal is to send the UGV to the exit from a certain space in the nursing home as soon as possible. The parameters of the UGV, the scenario and the neural network are assigned in Table 1. l represent the wheelbase of the vehicle respectively and N_d is the number of data in the data set.

Table 1. Vehicle/Algorithm-Related Parameters

Parameters	Values	Parameters	Values	Parameters	Values	Parameters	Values
l	0.5	$v^{\max}$	1	$\theta^{\max}$	180	N_d	200 000
$p_x^{\max}$	12	$a^{\max}$	0.75	$u_1^{\max}$	1	N_l	6
$p_y^{\max}$	8	$\phi^{\max}$	60	$u_2^{\max}$	2	N_n	64

Simulation comparisons are carried out to verify the effectiveness and accuracy of the proposed LSTMRDNN method. Fig. 2 shows the mission scenario of the UGV alongwith the comparison results of the optimal trajectory, the trajectory based on LSTMRDNN, DNN-based

method and MPC method. The trajectory optimization model (5) in this paper is addressed using the double-layer desensitization trajectory optimization method from [15] yielding the optimal trajectory for minimizing time in the present design scenario, serving as a reference for the theoretical optimum value. It can be observed that all four methods could complete the task safely and smoothly. Different performance of each methods was noticed. The trajectory obtained with the LSTMRDNN method almost overlapped with the optimal trajectory. The right side of Fig. 2 is the quantitative error evaluation curve of LSTMRDNN, DNN, MPC and the optimal trajectory. In order to judge the accuracy of the proposed method, we calculated the root mean square error (RMSE) of the actual value relative to the optimal value using the following formula:

$$RMSE(\boldsymbol{x}) = \sqrt{\frac{1}{N}\sum_{i=1}^{N_k}(\boldsymbol{x}_i^{\text{real}} - \boldsymbol{x}_i^{\text{opti}})^2} \tag{13}$$

where N_k represents the number of discrete points on the trajectory, $\boldsymbol{x}_i^{\text{real}}$ represents the state of the actual trajectory, and $\boldsymbol{x}_i^{\text{opti}}$ represents the state of the optimal trajectory.

The specific RMSE values obtained are shown in Table 2. The RMSE value of our proposed LSTMRDNN-based method is smaller than that of the MPC-based and DNN-based method.

Table 2. The RMSE Value of Each State Quantity

Method	p_x	p_y	v	a	θ	ϕ
The proposed	0.0209	0.0162	0.0094	0.0278	0.0110	0.0932
DNN	0.0317	0.0323	0.0115	0.0301	0.0168	0.1162
MPC	0.0395	0.0489	0.0160	0.0363	0.0288	0.1314

Furthermore, Fig. 3 illustrates the computation time for generating optimized trajectory control values using the trained LSTMRDNN network over 300 iterations. The computation time refers to the duration taken by the network to calculate corresponding control values

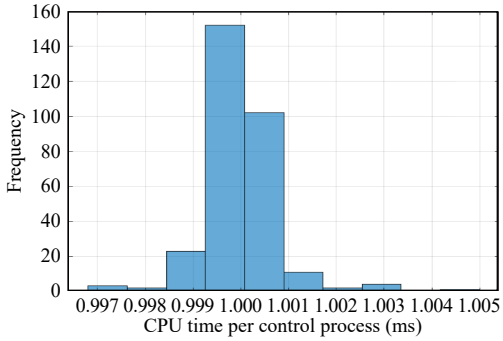

Fig. 3. Computation time for generating optimized trajectory control values using the trained LSTMRDNN network.

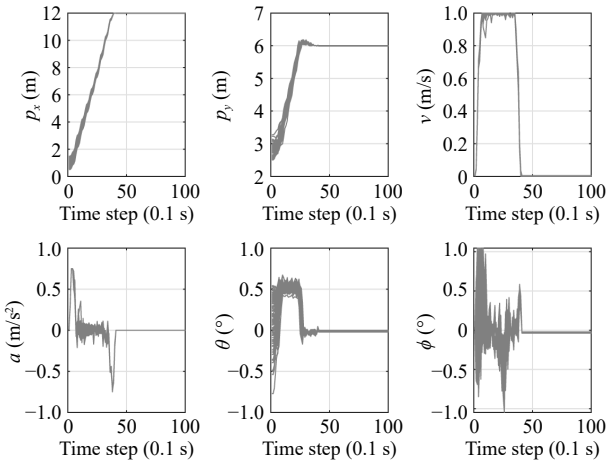

Fig. 4. Trajectory states change after reaching the target position.

after receiving the current state as input. As depicted in Fig. 3, the average computation time is approximately 1ms, indicating excellent real-time performance.

An experiment to test the stability of the proposed scheme was carried out subsequently. Fig. 4 shows the states set of the task track obtained with LSTMRDNN. It can be seen that even with the perturbations on initial state, the stability of the terminal state can be guaranteed.

Conclusion: In this letter, an LSTMRDNN-based trajectory optimization framework is proposed for the motion planning and control of UGVs. The performance and stability of the method is verified through theoretical analyses and experiments.

References

[1] R. Chai, A. Tsourdos, A. Savvaris, S. Chai, Y. Xia, and C. Chen, "Six-DoF spacecraft optimal trajectory planning and real-time attitude control: A deep neural network-based approach," *IEEE Trans. Neural Networks and Learning Systems*, vol. 31, no. 11, pp. 5005–5013, 2019.

[2] L. Chen, Y. Shan, W. Tian, B. Li, and D. Cao, "A fast and efficient double-tree RRT*-like sampling-based planner applying on mobile robotic systems," *IEEE/ASME Trans. Mechatronics*, vol. 23, no. 6, pp. 2568–2578, 2018.

[3] Y. Guo, D. Yao, B. Li, Z. He, H. Gao, and L. Li, "Trajectory planning for an autonomous vehicle in spatially constrained environments," *IEEE Trans. Intelligent Transportation Systems*, vol. 23, no. 10, pp. 18326–18336, 2022.

[4] B. Li, L. Li, T. Acarman, Z. Shao, and M. Yue, "Optimization-based maneuver planning for a tractor-trailer vehicle in a curvy tunnel: A weak reliance on sampling and search," *IEEE Robotics and Automation Letters*, vol. 7, no. 2, pp. 706–713, 2021.

[5] G. P. Kontoudis and K. G. Vamvoudakis, "Kinodynamic motion planning with continuous-time q-learning: An online, model-free, and safe navigation framework," *IEEE Trans. Neural Networks and Learning Systems*, vol. 30, no. 12, pp. 3803–3817, 2019.

[6] J. Fan, X. Chen, and X. Liang, "UAV trajectory planning based on bidirectional APF-RRT* algorithm with goal-biased," *Expert Systems With Applications*, vol. 213, p. 119137, 2023.

[7] J. Wang, J. Wang, and Q.-L. Han, "Receding-horizon trajectory planning for under-actuated autonomous vehicles based on collaborative neurodynamic optimization," *IEEE/CAA J. Autom. Sinica*, vol. 9, no. 11, pp. 1909–1923, 2022.

[8] Z. Wang, L. B. Freidovich, and H. Zhang, "Periodic motion planning and control for double rotary pendulum via virtual holonomic constraints," *IEEE/CAA J. Autom. Sinica*, vol. 6, no. 1, pp. 291–298, 2017.

[9] W. Hu, Z. Deng, D. Cao, B. Zhang, A. Khajepour, L. Zeng, and Y. Wu, "Probabilistic lane-change decision-making and planning for autonomous heavy vehicles," *IEEE/CAA J. Autom. Sinica*, vol. 9, no. 12, pp. 2161–2173, 2022.

[10] C. Sánchez-Sánchez and D. Izzo, "Real-time optimal control via deep neural networks: Study on landing problems," *J. Guidance, Control, and Dynamics*, vol. 41, no. 5, pp. 1122–1135, 2018.

[11] R. Chai, H. Niu, J. Carrasco, F. Arvin, H. Yin, and B. Lennox, "Design and experimental validation of deep reinforcement learning-based fast trajectory planning and control for mobile robot in unknown environment," *IEEE Trans. Neural Networks and Learning Systems*, 2022. DOI: 10.1109/TNNLS.2022.3209154

[12] K. J. Åström and B. Wittenmark, *Adaptive Control*. New York, USA: Dover Publications, 2008.

[13] K. Vamvoudakis, F. Lewis, and S. S. Ge, "Neural networks in feedback control systems," *Mechanical Engineers' Handbook*, pp. 1–52, 2014.

[14] D. Nodland, H. Zargarzadeh, and S. Jagannathan, "Neural network-based optimal adaptive output feedback control of a helicopter UAV," *IEEE Trans. Neural Networks and Learning Systems*, vol. 24, no. 7, pp. 1061–1073, 2013.

[15] R. Chai, A. Tsourdos, S. Chai, Y. Xia, A. Savvaris, and C. Chen, "Multiphase overtaking maneuver planning for autonomous ground vehicles via a desensitized trajectory optimization approach," *IEEE Trans. Industrial Informatics*, vol. 19, no. 1, pp. 74–87, 2022.